Photoinduced Intercomponent Processes in Selectively Addressable Bichromophoric Dyads Made of Linearly Arranged Ru(II) Terpyridine and Expanded Pyridinium Components

Fausto Puntoriero, Antonino Arrigo, Antonio Santoro, Giuseppina La Ganga, Fabien Tuyèras, Sebastiano Campagna, Grégory Dupeyre, Philippe P. Laine

Photoinduced intercomponent processes in selectively addressable bichromophoric dyads made of linearly-arranged Ru(II) terpyridine and expanded pyridinium components

Fausto Puntoriero,[a,*] Antonino Arrigo,[a] Antonio Santoro,[a] Giuseppina La Ganga,[a] Fabien Tuyèras,[b] Sebastiano Campagna,[a,*] Gregory Dupeyre,[b] and Philippe P. Lainé. [b,*]

[a] Department of Chemical, Biological, Pharmaceutical and Environmental Sciences (CHIBIOFARAM), University of Messina, and Centro Interuniversitario per la Conversione Chimica dell'Energia Solare (SOLAR-CHEM, sezione di Messina) – viale F. Stagno d'Alcontres 31, 98166 Messina, Italy.

[b] Univ Paris Diderot, Sorbonne Paris Cité, ITODYS, UMR CNRS 7086, 15 rue J-A de Baïf, 75013 Paris, France.

ABSTRACT

Three new linearly-arranged bichromophoric systems **1** – **3** have been prepared and their photophysical properties have been studied, taking also advantage of fs pump-probe transient absorption spectroscopy. The three compounds contain the same chromophores, that is a Ru(II)-terpy-like species and a fused expanded bipyridinium (FEBP) unit, separated by three different, variously methylated biphenylene-type brigdes. The chromophores have been selected to be selectively addressable and excitation involving the Ru-based or the FEBP-based dyes results in different excited-state decays. Upon Ru-based excitation at 570 nm, *oxidative* photoinduced electron transfer (OPET) takes place in **1** – **3** from the ^{3}MLCT state, however the charge-separated species does not accumulate, indicating that the charge recombination rate constant exceeds OPET rate constant. Upon excitation of the organic dye at 400 nm, the FEBP-based $^1\pi$–π^* level is prepared, which undergoes a series of intercomponent decay events, including (i) electron-exchange energy transfer leading to the MLCT manifold (SS-EnT), which successively decay according to 570 nm excitation, and (ii) *reductive* photoinduced electron transfer (RPET), leading to the preparation of the charge-separated (CS) state. Reductive PET, involving the FEBP-based singlet state, is much faster than oxidative PET, involving the MLCT triplet state, essentially because of driving force reasons. The rate constant of CR is intermediate between the rate constants of OPET and RPET, and this makes **1** – **3** capable to selectively read the 400 nm excitation as an active input to prepare the CS state, whereas excitation at wavelengths longer than 480 nm is inefficient to accumulate the CS state.

Moreover, intriguing differences between the rate constants of the various processes in **1** – **3** have been analyzed and interpreted according to the superexchange theory for electron transfer. This allowed to uncover the role of the electron-transfer and hole-transfer superexchange pathways in promoting the various intercomponent photoinduced decay processes occurring in **1** – **3**.

Introduction

Multicomponent systems integrating chromophoric and redox-active functional subunits are extensively investigated because of fundamental and potentially applicative reasons. For instance, multichromophoric species can be useful for light-harvesting purposes of relevance for light energy conversion and storage,[1] thereby contributing to gaining insights in great details into often intermingled photoinduced energy and electron transfer processes.[2]

In particular, linearly-arranged multifunctional assemblies, in which the chromophoric and redox-active subunits are covalently connected by semi-rigid, rod-like spacers, are quite appealing insofar as they allow (i) studying various intercomponent photoinduced energy and electron transfer processes and (ii) sheding light on the role of the spacers in the mechanism – including rates and efficiencies – of the various decay processes.[2] When the chromophores can be selectively excited at different wavelengths as a result of a proper combination of subunits, interesting behavior are likely to take place, that can be rationalized within the framework of the conceptual corpus of Supramolecular Photochemistry.[2a,3] A typical example is the possibility of preparing a charge-separated (CS) state via different pathways and on different timescales; in some circumstances, molecular design should make it possible accumulation of such a CS state at specific wavelengths only, that is, on exciting only a chromophoric subunit. Such a behavior would be an example of a *programmed* system,[4] featuring different properties depending on the wavelength of the absorbed light (the wavelength at which the CS state can be formed would be the *readable* input, capable to activate the program embedded in the system, whereas excitation of the second chromophore would be inefficient to activate the function), still in the presence of quite efficient intercomponent energy and electron transfer processes.[5]

Furthermore, charge separation obtained by *oxidative* or *reductive* photoinduced electron transfer in linearly-arranged, rigid bichromophoric species is suitable to explore the superexchange theory for electron transfer as well as for Dexter energy transfer (based on a

double electron exchange), all the more when a series of closely related assemblies is available.[2d,2f,2g,2i,2k,6-8] New insights into superexchange-mediated photoinduced electron transfers have been recently introduced, with special emphasis placed on the observation that some virtual states normally expected to mediate charge recombination were however found to be inoperative for certain photoinduced charge separation processes, depending on the *oxidative* or *reductive* nature of the excited-state process.[6,7] This situation is likely to allow preparation of long-lived CS states using preferably one route rather than the other (i.e., exciting the *donor* or the *acceptor* chromophoric subunit), as a function of the nature of the spacer.

We have recently introduced a class of species referred to as *branched* or *fused* expanded (bi)pyridiniums that display appealing photophysical, electronic and redox properties (multifunctional entities).[9,10] These molecules can serve as functional building blocks of multicomponent assemblies insofar as they feature a phenylene or biphenylene terminus as a pendant proto-spacer. In fact, these pyridinium-based species primarily act as electron acceptor subunits owing to their reversible electrochemical behavior, their reduction occurring at mild potentials (i.e. less negative than -1.00 V vs SCE in acetonitrile solution). We selected the *fused* expanded bipyridinium species out of the previously studied family and prepared three new bichromophoric species (molecular dyads) in which the well-known Ru(II) bis-terpy chromophore (terpy = 2,2':6',2"-terpyridine) is connected to an expanded, fused bipyridinium chromophore (herein denoted as FEBP) by means of different methyl-decorated *p*-biphenylene subunits about their interannular linkage, as variably twisted rigid, linear spacers. The studied compounds **1** – **3** are shown in **Figure 1**, together with the structural formulae of reference chromophores including the inorganic model species $Ru(tterpy)_2^{2+}$ (**M**) (tterpy = 4'-*p*-tolyl-2,2':6':2"-terpyridine) and five FEBP-based organic chromophores differentiated by both their pendant mono- or bi-phenylene termini as well as their methyl (Me) decoration patterns. All the cationic species here studied are hexafluorophosphate salts.

The FEBP chromophoric core (**L0** and **L1** in Figure 1) of **1** – **3** has been selected because it absorbs significantly in the 350 – 450 nm spectral region,[9b] where the inorganic photosensitizer absorbs only weakly, and conversely: this FEBP core does not absorb appreciably above 460 nm, where the ruthenium unit exhibits its intense spin-allowed metal-to-ligand charge-transfer (MLCT) band, in the 460 – 550 nm region. This allows to selectively excite the two chromophores of the **1** – **3** series of dyads.

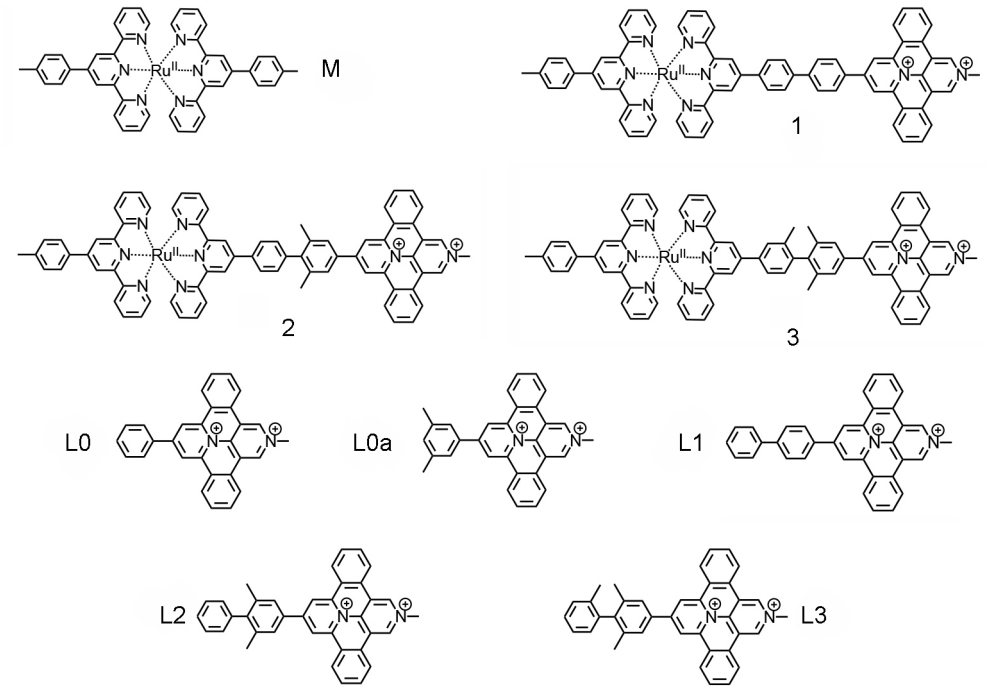

Figure 1. Structural formulae of the bichromophoric species **1** – **3** here studied and of their reference compounds **M**,[1a] **L1**,[9b,9d] **L2**,[9d] **L3**[9d] (biphenylene-containing dyes), and the phenylene-containing organic dyes **L0**[9b] and **L0a**.[9d]

Results and Discussion

Synthetic strategy. The general synthetic strategy to obtain the inorganic compounds **1**–**3** is given in the Supporting Information (Schemes in Page S5). It is worth noticing here that, as previously stated,[9e] ligands bearing a fused expanded pyridinium must be prepared before carrying out coordination chemistry (i.e., strategy based on "photochemistry on the complex",

with dyads built from branched expanded pyridiniums is not operative). The terpyridine ligands with appended expanded bipyridinium components (i.e., the ligands in **1**–**3**) were thus synthesized by Suzuki coupling of the suitable chelating aryl-tpy fragments bearing a boronic ester moiety with diverse brominated dibenzoquinolizinonaphthyridinium derivatives (themselves obtained by photochemical pericondensation of branched expanded pyridiniums according to routes previously described).[9d] The boronic ester derivative "neoB-tol-tpy" needed for synthesis of the ligand in **3** was previously prepared by condensation of 2-acetylpyridine with 4-bromo-3-methylbenzaldehyde in presence of ammonia and subsequent Miyaura borylation of the resulting brominated tpy derivative with bis(neopentylglycolato)diboron. Resulting tpy-expanded bipyridinium ligands were then engaged in a metalation step by reacting with [(tterpy)$RuCl_3$], and a final quaternization step using MeOTf as methylating agent allowed synthesis of the target bispyridinium dyads **1**–**3**.

Redox behavior. The molecular dyads **1** – **3** here studied show a reversible one-electron oxidation process and several reversible one-electron reduction processes. Data are gathered in **Table 1**. The oxidation potential is straightforwardly assigned to a process involving the metal center of the photosensitizer,[11] while the reduction processes are ligand-centered.[7c,9e,11] Among these processes, only the first reduction is relevant here, which is ascribed to the bipyridinium unit, by comparison with the model compounds.[9b,9d] It is worth noting that both oxidation and reduction potentials in the dyads are essentially the same as those measured for reference species **M** and **Ln** (**Figure 1**).[1a,9b,9d] This observation indicates that, in the dyads, electronic and electrostatic interactions between the two positively charged redox-active units at the ground state are virtually negligible from an electrochemical point of view.

Table 1. *Redox data of the studied compounds and of some of their reference species, in acetonitrile. Only the first oxidation and reduction potentials are reported.*[a]

compound	$E_{1/2\,(ox)}$, V vs SCE	$E_{1/2\,(red)}$, V vs SCE
M	+ 1.22	- 1.27
1	+ 1.23	- 0.42
2	+ 1.23	- 0.43
3	+1.22	-0.45
L1[b]		-0.42
L0[b]		-0.43

(a) $E_{1/2}$ (vs SCE) is calculated as (E_{pa} + E_{pc}) /2, where E_{pa} and E_{pc} are the anodic and cathodic peak potentials measured by cyclic voltammetry at 0.1 V s^{-1}. The experiments are made at platinum electrode, using 0.1 M NBu_4PF_6 as supporting electrolyte. (b) Data from ref. **9b**.

Absorption spectra. The absorption spectra of **1** – **3** and their model species **M** and **L** in acetonitrile solution (see **Figure 2** and **Figure S1** in the *Supporting Information*) exhibit intense bands in the UV region, due to ligand-centered (LC) transitions, and relatively intense bands in the visible region attributed to spin-allowed MLCT transitions involving the Ru(II) and the two terpyridine-based ligands. The FEBP organic dye (typically represented by **L0** model molecule in **Figure 1**) has an absorption spectrum featuring intense, structured bands in the 350 – 450 nm region (see **Figure 2**)[12] and some contributions at shorter wavelengths. A cursory look at **Figure 2** and at the data in **Table 2** clearly indicates that the individual chromophores of **1** – **3** keep their spectroscopic integrity within the molecular dyads: in particular, the low-energy, visible part of the absorption spectrum of the complexes is exclusively due to the spin-allowed MLCT band, whereas the structured band in the 350 – 450 nm region mostly originates in transitions involving the FEBP chromophore. So, as mentioned in the introduction section, the two chromophores of **1** – **3** are amenable to be selectively addressed.

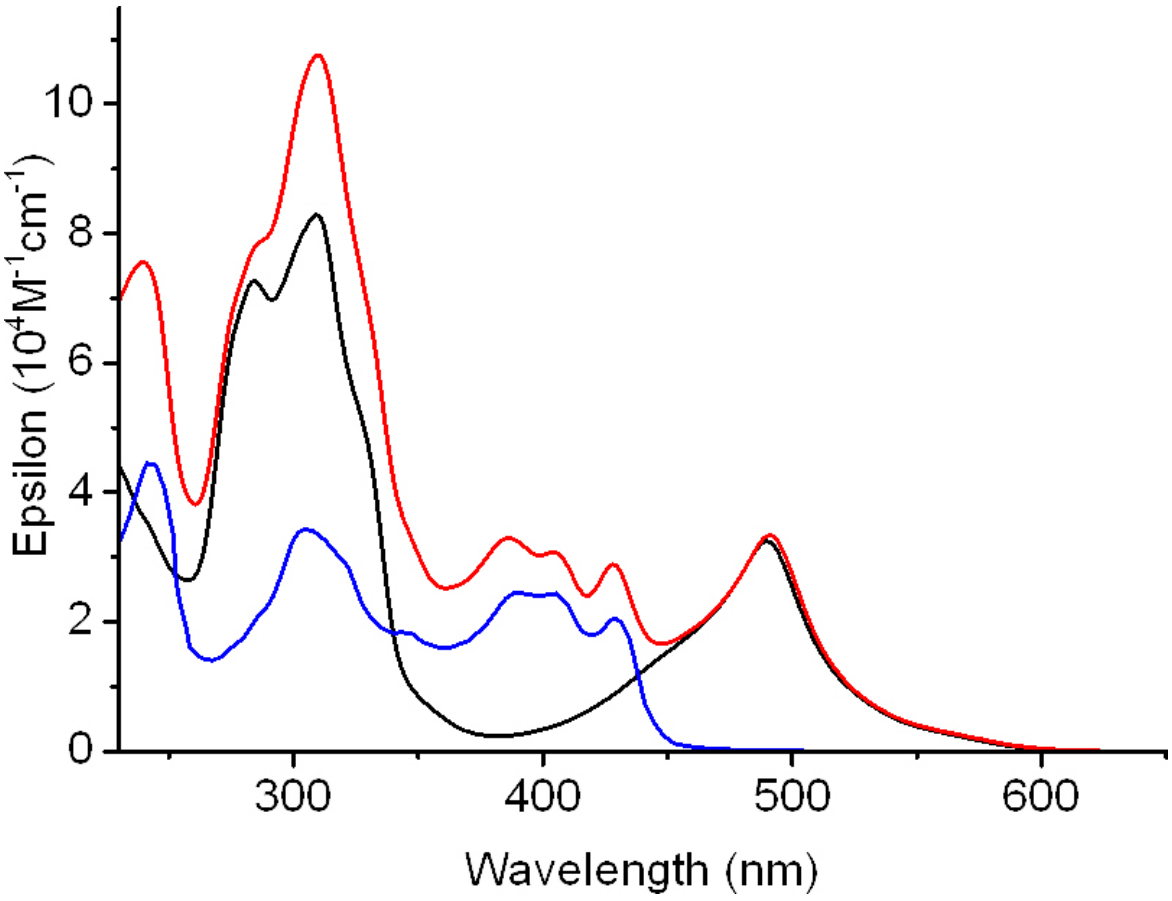

Figure 2. Absorption spectra of some representative compounds in acetonitrile solution. The panel shows the absorption spectra of the "free" chromophore dye missing the metal subunit **L3** (blue line), of **3** (red line) and of **M** (black line).

Luminescence. Both **M** (inorganic chromophore) and **L** model species (Figure 1) exhibit luminescence at room temperature in fluid solution and at 77 K in rigid matrix (see **Table 2**).[9b] **M** has the typical ^{3}MLCT emission of Ru(II) polypyridine complexes,**11** whereas the biphenylene-(methyl-decorated) organic units, **Ln**, exhibit fluorescence from their $^1\pi$–π^* level at about 430 nm and phosphorescence in the range 490-540 nm at 77 K rigid matrix.[9b,9c] At room temperature, in **L1**, a CT state involving the biphenylene subunit as the donor and the positively-charged FEBP fragment as the acceptor is stabilized and CT emission takes place at about 600 nm.[9b] Similar behaviors are reported for **L2** and **L3**.[9d]

Table 2. Absorption spectra and luminescence data.[a]

	Absorption[b]	Luminescence, 298 K			Luminescence, 77 K	
Compound	λ_{max} / nm (ε / M^{-1} cm^{-1})	λ_{max} / nm	τ / ns	Φ	λ_{max} / nm	τ / μs
1	493 (37 000)	*not emissive*			636	13.7
2	492 (37 000)	*not emissive*			628	12.4
3	492 (32 000)	*not emissive*			628	11.1
M	492 (31 800)	648	1.0	3.2×10^{-5}	628	12.5
L1[c]	428 (40 700)	610	2.8	0.10	430 540	3.5×10^{-3} 175×10^{3}
L2[d]	427 (30 200)	567	3.7	0.22	436 500	4.2×10^{-3} 150×10^{3}
L3[d]	427 (20 300)	565	3.4	0.12	433 498	4.8×10^{-3} 498×10^{3}
L0[c]	428 (22 200)	453	4.1	0.22	434 494	5.1×10^{-3} 430×10^{3}
L0a[d]	428 (21 400)	463	3.1	0.28	434 505	5.9×10^{-3} 610×10^{3}

(a) Data in acetonitrile solution, except for luminescence data at 77 K, that have been obtained in butyronitrile rigid matrix for **M** and **1** – **3** and in MeOH/EtOH 4.1 (v/v) for **L0** – **L3** and **L0a**. For the latter species, both fluorescence and phosphorescence occur at 77 K. (b) Only the maximum of the lowest-energy absorption band is given. (c) Data from **ref. 9b**. (d) Data from **ref. 9d**.

A better model for the excited-state properties of the fused expanded bipyridinium subunit (FEBP), not involving CT states, is probably **L0**, in which the pendant proto-spacer is a mere phenylene group instead of the electron-donating biphenylene group (**L1**). For this species, a π–π* singlet state is responsible for the room temperature emission, peaking at 453 nm.[9b] Analogous results are also reported for compound **L0a**, containing a pendant dimethyl-substituted phenylene (i.e. mesithylene) instead of tilted biphenylene groups of **L2** and **L3**.[9d]

As usual for Ru(II) complexes with tridentate, terpy-like ligands, the room temperature ^{3}MLCT emission of **M** is very weak and short-lived (see data in **Table 2**), due to a thermally-activated surface crossing from the emissive ^{3}MLCT state to the closely-lying ^{3}MC (metal centered) level, which promotes fast radiationless decay to the ground state.[1a,11] However, the weak emission of the model **M** is totally absent in **1** – **3** at room temperature, indicating the presence of a further quenching process of the ^{3}MLCT excited state. At 77 K, the thermally-activated decay process via the ^{3}MC state is not available, and **M** shows a relatively long-lived ^{3}MLCT emission. In this condition, also **1** – **3** exhibit an emission quite similar to that of **M**, indicating that the further quenching process that occurs at room temperature is no longer operative at 77 K also in **1** – **3**.

Even by exciting at 400 nm, where the organic chromophores are selectively addressed, **1** – **3** do not exhibit any luminescence at room temperature, thus indicating that the potentially emissive CT state of the FEBP subunits is quenched or, most likely, that the singlet π–π* level from which the CT state is formed decays via a different and more efficient pathway, most likely via an energy transfer to the MLCT state. In fact, no luminescence except the MLCT emission is recorded at 77 K, at any excitation wavelength. This finding indicates that an energy transfer from the organic dye to the metal-based subunit takes place in this condition. This makes clear why **L0** and **L0a** (where CT states are not present) are assumed to be better models than **L1 - L3** for the excited state properties of the biphenylene-type bridges in **1 - 3**.

To investigate in detail the excited-state decay processes occurring in the bichromophoric systems **1** – **3**, pump-probe transient absorption spectroscopy was employed (see below).

Pump-probe transient absorption spectra and photoinduced intercomponent processes. Our first aim was to understand the reason for the quenching of the ^{3}MLCT emission of metal complex subunits in **1** – **3** in fluid acetonitrile solution at room temperature. Indeed, oxidative

photoinduced electron transfer (OPET) that involves the ^{3}MLCT state of the dyads (with the metal-based chromophore acting as the light-trigerred donor) and the FEBP subunit as the acceptor is thermodynamically allowed by ca 0.30 eV, according to eqs. 1 and 2, in which all the energy terms are expressed in eV.

$$\Delta G^0_{OPET} = e(^*E_{oxRu} - E_{redFEBP}) + W \quad (1)$$

$$e^*E_{oxRu} = eE_{oxRu} - E^{0\text{-}0}_{Ru} \quad (2)$$

In eq. 1, ΔG^0_{OPET} informs on the driving force for the oxidative, photoinduced electron transfer, e is the electron charge, $^*E_{oxRu}$ is the oxidation potential of the ^{3}MLCT excited state, in its turn approximated from eq. 2, where E_{oxRu} is the ground state oxidation potential of the Ru-based unit, $E^{0\text{-}0}_{Ru}$ is the ^{3}MLCT excited state energy - assumed as the ^{3}MLCT emission maximum at 77 K - and $E_{redFEBP}$ is the reduction potential of the FEBP bipyridinium acceptor.[13] The relevant redox potentials and excited state levels are given in **Tables 1** and **2**. The work term, indicated with W, which represents the difference between Coulombic stabilization energies of reactants and products, is neglected as a first approximation. Pump-probe transient absorption spectroscopy of the molecular dyads **1** – **3** (**Figure 3**), performed on exciting at 570 nm where only the metal-based subunits of the dyads absorb, gave transient spectra quite similar to one another, practically also identical to that of **M**; they are characterized by a bleaching around 490 nm, corresponding to the ^{1}MLCT absorption band of the ground state species, and a broad transient absorption spanning the red portion of the visible spectrum, assigned to absorption of the reduced – and planarized – phenyl-terpyridine fragment.[14] In all cases, the excited state formed is assumed to be the ^{3}MLCT state (intersystem crossing from the initially populated ^{1}MLCT level is known to be extremely fast, occurring in less than 100 fs,[15] and is probably complete within the laser pulse), which decays to the ground state without any intermediate, as indicated by the isosbestic point that for all **1** – **3** is at $\Delta A = 0$. The only difference between the TAS of **M** and **1** – **3** is the decay time constant, that is reduced from 1 ns (**M**) to 40 ps, 173 ps, and 360 ps, for **1, 2**, and **3**,

respectively. Assuming electron transfer as the reason for MLCT quenching, these values yield rate constants of 2.4×10^{10} s^{-1}, 4.8×10^{9} s^{-1}, and 1.8×10^{9} s^{-1} for the photoinduced oxidative charge separation process occurring in **1**, **2**, and **3**, respectively.

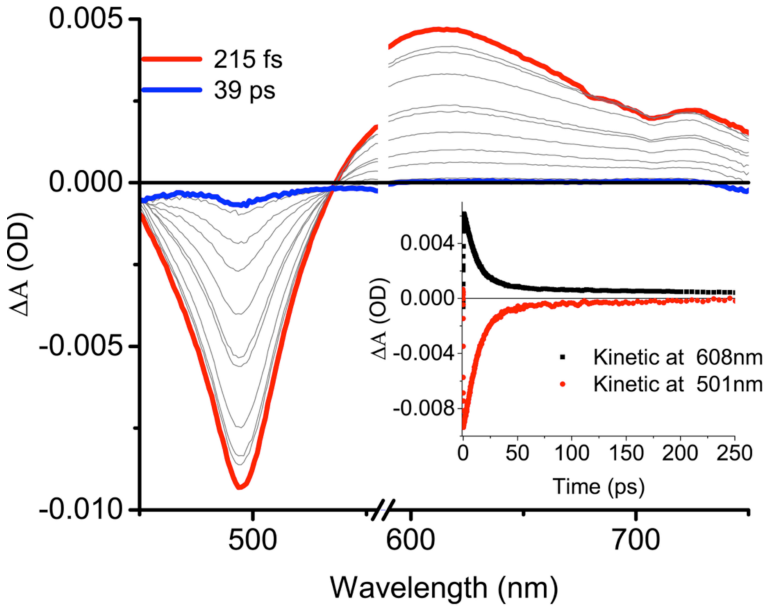
0.005
0.000
-0.005
-0.010
ΔA (OD)
215 fs
39 ps
0.004
0.000
-0.004
-0.008
ΔA (OD)
Kinetic at 608nm
Kinetic at 501nm
0
50
100
150
200
250
Time (ps)
500
600
700
Wavelength (nm)

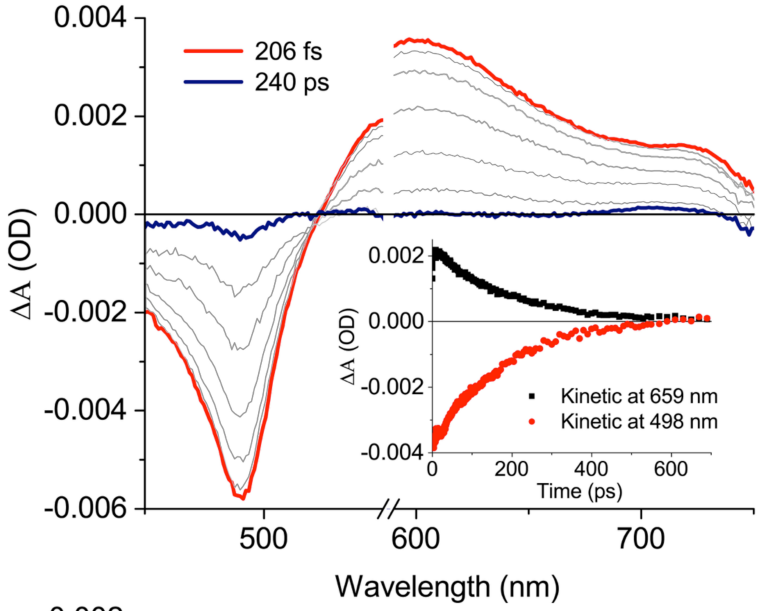
0.004
0.002
0.000
-0.002
-0.004
-0.006
ΔA (OD)
206 fs
240 ps
0.002
0.000
-0.002
-0.004
ΔA (OD)
Kinetic at 659 nm
Kinetic at 498 nm
0
200
400
600
Time (ps)
500
600
700
Wavelength (nm)

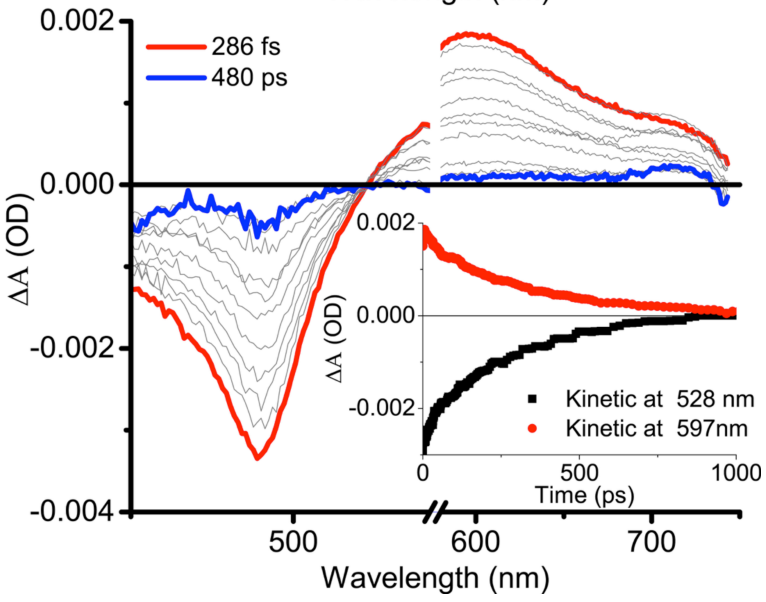
0.002
0.000
-0.002
-0.004
ΔA (OD)
286 fs
480 ps
0.002
0.000
-0.002
ΔA (OD)
Kinetic at 528 nm
Kinetic at 597nm
0
500
1000
Time (ps)
500
600
700
Wavelength (nm)

Figure 3. Transient absorption spectra and decays of **1** (top panel), **2** (middle panel) and **3** (bottom panel), in acetonitrile upon excitation at 570 nm. All the spectra were cutted in the range between 560 nm and 585 nm because of the excitation pulse signal. The spectra at wavelengths longer than 585 nm are magnified for clarity purposes.

The above calculated values of photoinduced charge separation (CS) rates well agree with superexchange theory,[8,16] that implies that photoinduced *oxidative* electron transfer in donor-bridge-acceptor dyads is governed by the electron-transfer route, i.e. depends from the energy of LUMO orbitals extension on the bridges.[6b] In fact, reduction potentials become slightly more negative on passing from biphenylene to the methyl substituted analogues, which indicates that the FEBP-centered LUMO is destabilized such that the superexchange-mediated electronic coupling via the electron-transfer route between donor and acceptor decreases along the series **1, 2**, **3**, thereby justifying the decrease of charge separation rate constants. However, it should be noted that superexchange also takes into account electronic interactions due to coupling factors that depends on geometrical factors, and such coupling factors also foresee the decrease of the electronic matrix element, and therefore of electron transfer rate constants, along the series **1, 2, 3**. This indicates that electronic factors, beside energy considerations, contribute to the difference in charge separation rate constants in the series.

The absence of any intermediate in the TAS spectra – in particular, the lack of increased absorption at around 530 nm, which is the fingerprint of FEBP reduced form[9e] – indicates that charge recombination is faster than oxidative photoinduced charge separation in **1** – **3**, thus impeding accumulation of the charge-separated states. This is in line with other reported results obtained for molecular dyads involving Os(II) polypyridine compounds and related electron acceptors.[7c,9e,17] Their behavior was explained by considering that biphenylene bridging ligands are relatively easy to oxidize, so that the back electron transfer process (i.e., the charge recombination process) takes the form of hole transfers via low-lying virtual states

involving the HOMO extension on the bridge. This pathway, that cannot be borrowed for the forward OPET process, precludes long-lived charge separation.[6]

Transient absorption decays of **1** – **3** are much more complex when the dyads are excited at 400 nm, that is, at a wavelength at which excitation essentially – although not exclusively – involves the FEBP organic chromophore (for instance, compare absorption spectra of the individual components and of the dyad **3** in **Figure 2**). The complete 3D matrices of the TAS experiments of **M** and **1** – **3** are shown in the *Supporting Information* (**Figure S2**). The **1** – **3** dyads behave qualitatively in the same way, the only difference being, as for the excited state decay obtained upon excitation at 570 nm, the time constants of the various processes. For **1** – **3**, decay is multiphasic: as a representative example, we here discuss the case of compound **3** in detail.

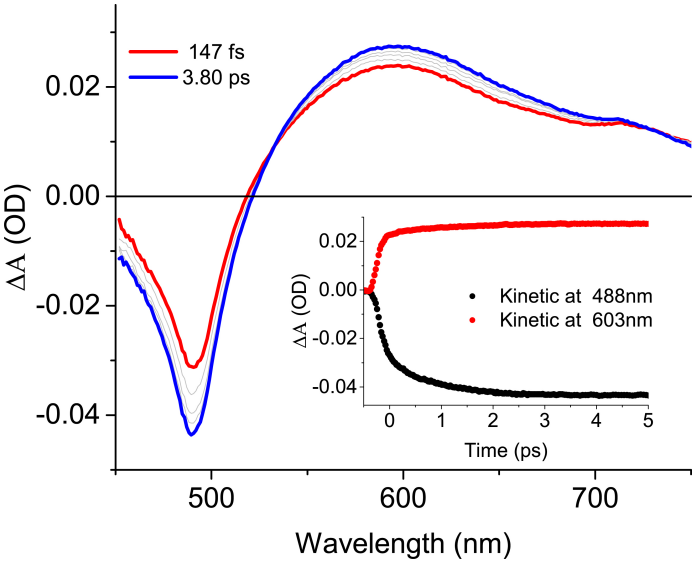

Figure 4. Transient absorption spectra of dyad **3** in acetonitrile, referred to as the first process, upon excitation at 400 nm. In the inset, kinetic decays in the bleaching minimum at λ = 488 nm and in the transient absorption band maximum at λ = 603 nm are shown.

Figure 4 shows the early times of the excited state decay of the TAS of **3**, upon 400 nm excitation. Of note, the initially-prepared transient spectrum evolves, featuring an increase of the spectral bleaching that peaks at about 490 nm, as is also the case for the red-edge transient absorption band, which is straightforwardly assigned to the reduced phenyl-terpyridine. This

evolution occurs with a time constant of 1.1 ps for **3** and is accompanied by the presence of an isosbestic point at $\Delta A \neq 0$, at about λ = 537 nm. These observations show that the running process involves a state different from the ground state. These changes indeed indicate that population of the singlet MLCT state is increasing, as revealed by the further bleaching at 490 nm and the accompanying further raise of the lower energy transient absorption. Therefore this process can be reasonably assigned to a singlet-singlet energy transfer from the excited state of the organic acceptor (which absorbs the main fraction of the excitation light and is directly prepared upon laser pulse) to the ^{1}MLCT level of the Ru-based subunit, which then very rapidly undergoes intersystem crossing to ^{3}MLCT.[15] Note that the same process occurs in **1** and **2**, but the time constants in those cases are 105 fs and 570 fs, respectively. The driving force for singlet-singlet energy transfer is about 0.34 eV, assuming (i) the 77 K fluorescence emission of **L0a**, 434 nm,[9d] as the energy of the singlet state of the FEBP dye and (ii), the singlet MLCT level at the maximum of the absorption band (492 nm).[18]

Further data analysis reveals a second process, characterized with an isosbestic point which shifts to a different wavelength (around 540 nm), again with a $\Delta A \neq 0$ (see **Figure 5**). The new transient spectra feature a peculiar absorption increase contributing at around λ = 530 nm, which is the fingerprint of the formation of the reduced form of FEBP-type species, as previously demonstrated.[7c,9e] Therefore, even for the case of **3**, the transient absorption contribution can be assigned to the formation of the reduced form of the FEBP organic dye, and the second process is identified as a photoinduced, *reductive* charge separation, in which one electron is transferred from the metal-based subunit to the excited FEBP subunit. This process occurs with a time constant of 12 ps. A similar process also takes place in **1** and **2,** with time constants of 8.0 ps and 8.6 ps, respectively. The ΔG for such reductive photoinduced electron transfers ($\Delta G^0_{\mathrm{RPET}}$) can be calculated by using eqs. 3 and 4, that correspond to eqs. 1 and 2, discussed for the case of photoinduced, oxidative electron transfer.

$$\Delta G^0_{\mathrm{RPET}} = \mathrm{e}(E_{\mathrm{ox}Ru} - {}^{*}E_{\mathrm{red}FEBP}) + W \qquad (3)$$

$$e^*E_{redFEBP} = eE_{redFEBP} - E^{0\text{-}0}{}_{FEBP} \quad (4)$$

As in eqs.1 and 2, *e* is the electron charge, *W* is the work term, neglected here, and the other terms have specular meanings to those in eqs 1 and 2: $^*E_{red\ FEBP}$ is the reduction potential of the $^1\pi$–π^* FEBP-based excited state – in its turn approximated from eq. 4, where $E_{redFEBP}$ is the ground state reduction potential of the FEBP-based unit, and $E^{0\text{-}0}{}_{FEBP}$ is the $^1\pi$–π^* FEBP-based excited state energy, assumed as the fluorescence maximum at 77 K – and E_{oxRu} is the oxidation potential of the metal-based subunit. By using eqs 3–4 and the data in **Tables 1**–**2**, ΔG^0_{RPET} is -1.06 eV for **1** and -1.18 eV for **2** and **3**.

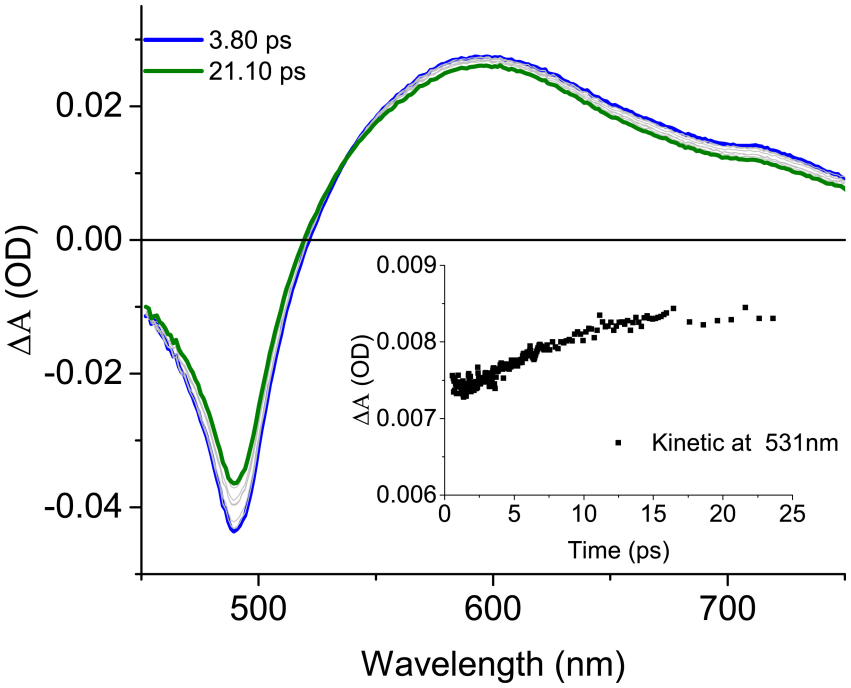

Figure 5. Transient absorption spectra of **3** in acetonitrile (excitation, 400 nm), referred to as the second process. In the inset, the kinetic decay at λ = 531 nm is shown, in correspondence with the rising transient absorption band. The decay also shows longer times.

After the second process, the isosbestic point moves again to a different wavelength (525 nm), indicating that a third process is occurring (see **Figure 6** and the decay curve in the inset of **Figure 5**). The third process is characterized by the disappearing of the small contribution at 531 nm, indicating that the charge-separated excited state is decaying via the charge

recombination process. This latter process occurs with a time constant of 32 ps in **3.** The corresponding process in **1** and **2** occurs with time constants of 15 ps and 32 ps, respectively. Charge recombination driving force, on the basis of the data in **Tables 1** – **2** and eqs. **3** – **4**, is 1.67 eV for **1** and 1.66 eV for **2** and **3**.

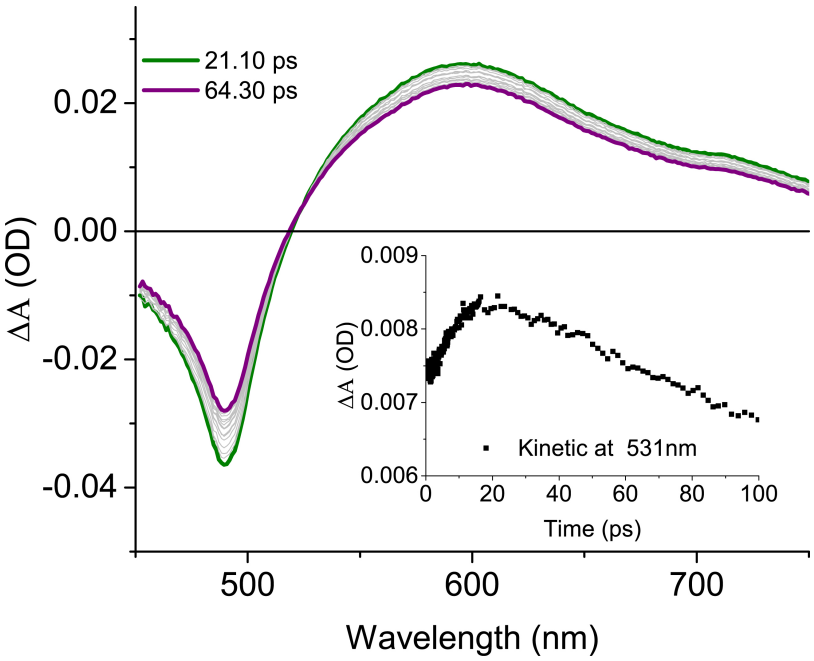

Figure 6. Transient absorption spectra of **3** in acetonitrile, referred to as the third process in the text. In the inset, the kinetic decay is showed at λ = 531 nm, in correspondence with the transient absorption band due to the reduced acceptor.

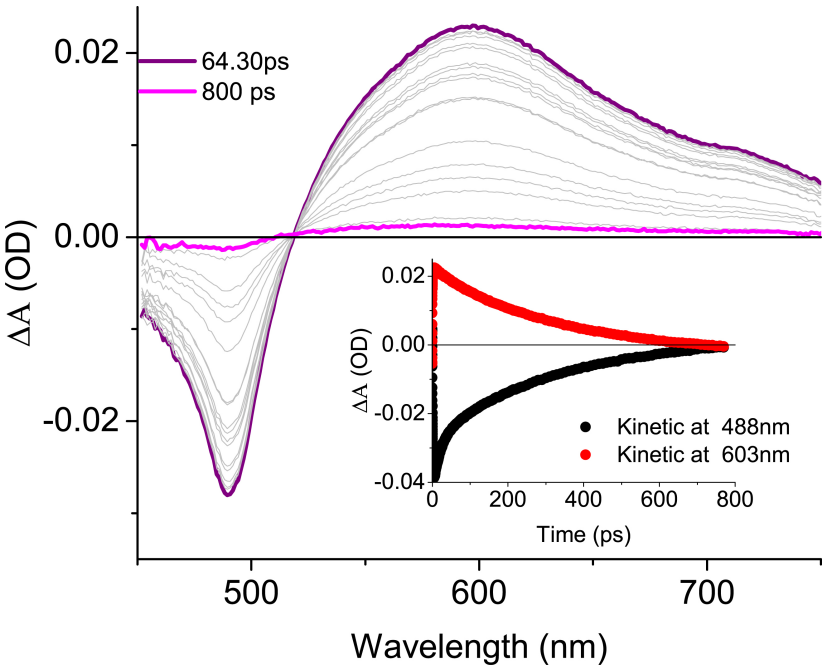

Figure 7. Transient absorption spectra of dyad **3** in acetonitrile, referred to as the fourth process discussed in the text.

Finally, the transient spectrum decays to the ground state by a slower process (time scale, 360 ps in **3**) as indicated by the isosbestic point associated with this process, which is at $\Delta A = 0$ for $\lambda = 520$ nm. This final process is shown in **Figure 7**. Interestingly, this process coincides with the TAS decay of **3** when excited at 570 nm, that is by exciting the metal-based chromophore, and can be assigned to an *oxidative* photoinduced electron transfer (OPET) involving the ^{3}MLCT excited state. Thus, this CS state can either be generated directly by the excitation laser light (a small percentage of the 400 nm exciting light is indeed also absorbed by the metal subunit; see **Figure 2**) or it can be produced following a singlet-singlet energy transfer from the initially-prepared FEBP-based excited state, which is the first process recorded upon 400 nm excitation. For compounds **1** and **2**, the time constants of the fourth process are respectively 45 ps and 175 ps, also in agreement with the photoinduced charge separation from the MLCT state assessed above upon excitation at 570 nm (40 ps and 173 ps for **1** and **2**, respectively). Clearly, the charge-separated state cannot be accumulated via

photoinduced *oxidative* electron transfer, as previously discussed, so photoinduced *oxidative* electron transfer apparently directly leads to the ground state.

The excited-state decay of **3** upon 400 nm excitation is summarized in **Figure 8**.

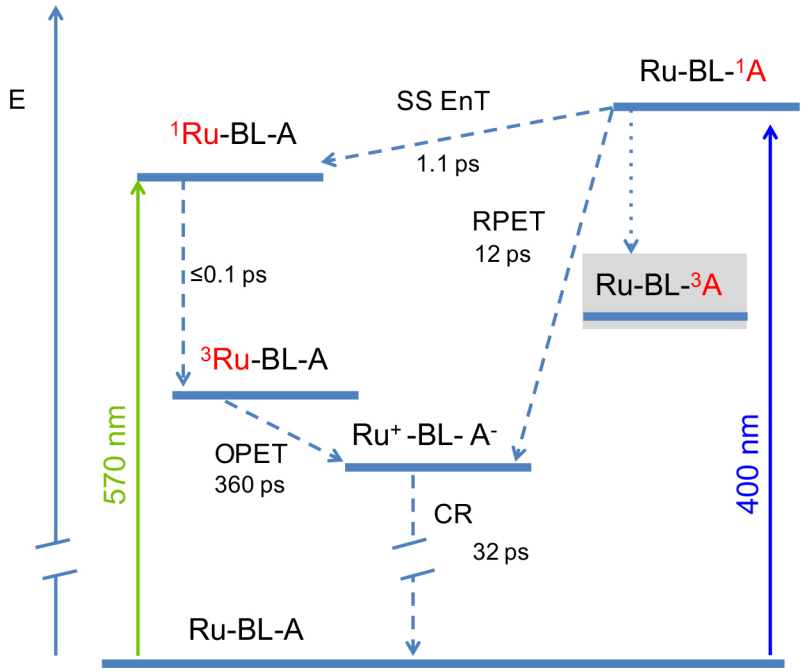

Figure 8. Schematization of the excited-state decay of **3**. In the schematization, Ru stands for the metal-based chromophore and A stands for the FEBP organic dye. BL is the biphenylene-type spacer. SS EnT stands for singlet-singlet energy transfer; RPET and OPET are reductive and oxidative photoinduced electron transfers, respectively, CR is charge recombination (or back electron transfer). The triplet Ru-BL-^{3}A state is highlighted in grey to indicate that most likely it is not formed because intersystem crossing within the organic dye subunit cannot compete with the intercomponent processes. The excited subunit is indicated by the red color. Noteworthy, upon excitation at 570 nm only the process related to OPET is observed.

Table 3. ΔG values and time constants of the various processes occurring in **1-3** in acetonitrile fluid solution, obtained by transient absorption spectroscopy.[a]

Dyad	SS-EnT	RPET		CR		OPET	
	τ	ΔG^0_{RPET}	τ	ΔG^0_{CR}	τ	ΔG^0_{OPET}	τ
1	105 fs	− 1.06 eV	8.0 ps	− 1.67 eV	15 ps	− 0.30 eV	40 ps
2	570 fs	− 1.18 eV	8.6 ps	− 1.66 eV	32 ps	− 0.31 eV	173 ps
3	1.1 ps	− 1.18 eV	12 ps	− 1.66 eV	32 ps	− 0.30 eV	360 ps

(a) SS-EnT is singlet-singlet energy transfer from the singlet FEBP-based excited state to the ^{1}MLCT level. CR is charge recombination. The other terms have meanings already introduced in the paper. ΔG for SS-EnT process is -0.34 eV for all the complexes.

Table 3 summarizes the time constants of the various decay processes occurring in **1** – **3**. Comparison between the various rate constants obtained for the same process in the various species warrants a detailed discussion. Before going into detail of a specific process, however, it is useful to realize that the reorganization energy of the various electron transfer processes should be quite similar moving along the series of compounds, so the difference in rate constants can mainly be related to electronic coupling.

Singlet-singlet energy transfer (SS-EnT). The experimental results indicate that such a process is the fastest decay process of the singlet excited state of the FEBP-based organic chromophore in **1** – **3** (**Table 3**). Moreover, the time constant decreases on passing from **1** to **3**. Considering that the donor-acceptor separation between the components is identical throughout the series, and that the spectral overlaps are similar, and the same holds for driving force, as well as for the photophysical properties of both of the donor and acceptor isolated subunits (that are basically common to all the members of the series), the fact that the time constants are different is an indication in favor of Dexter electron-exchange energy transfer as the dominant mechanism for the process. Indeed, calculation of Förster energy transfer according to the simplified equations **5** and **6** yield energy transfer rate constants of 35.6 ps, 11.4 ps, and 19.2 ps for **1**, **2**, and **3**, respectively, in all cases much slower than experimental data (**Table 3**), definitely indicating that SS-EnT occurs via Dexter mechanism.[19]

$$J_F = \frac{\int F(\bar{\nu})\varepsilon(\bar{\nu})/\bar{\nu}^4 \, d\bar{\nu}}{\int F(\bar{\nu}) d\bar{\nu}} \qquad (5)$$

$$k_{en}^{F} = 8.8x10^{-25} \frac{K^2 \Phi}{n^4 r_{AB}^6 \tau} J_F \qquad (6)$$

Dexter energy transfer can be discussed, as electron transfer, within the frame of the superexchange theory (it should be recalled, however, that reorganization energy for energy transfer is usually much smaller than for electron transfer). Within this frawework, in covalently-linked donor-acceptor systems, the electronic coupling between donor and acceptor depends on the spacer (or bridging ligand); assuming that the main mechanism for electronic coupling via superexchange between the dyes of **1** – **3** is dominated by the electron-transfer route, the presence of hindering methyl substituents within the spacers of **2** and **3** destabilizes the LUMO extension on the spacer with respect to **1** (geometrical decoupling), making smaller the superexchange-mediated electronic coupling, and as a consequence slower the energy transfer, on going from **1** to **2** and **3**. Once formed, the ^{1}MLCT undergoes ultrafast (<100 fs) intersystem crossing, leading to ^{3}MLCT, as already mentioned.

Oxidative photoinduced electron transfer (OPET). As is the case for SS-EnT, the OPET process becomes slower on going from **1** to **3** (**Table 3**). The reason would be the same, too: the electron transfer mechanism would indeed be assumed to be a superexchange-mediated one. The electron-transfer pathway involves the lowest-lying virtual MO of the bridging ligand, which also ensures the coupling between the extension of the FEBP-centred LUMO and vicinal unoccupied orbitals of the metal-based moiety. This coupling is a function of the interannular torsional angle of the spacer and is governed by the methyl-substitution pattern of the biphenylene linker. In principle, a hole-transfer pathway could also contribute to the process, but the virtual states involved in the hole-transfer pathway for OPET would require a simultaneous two-electron movement or a quite high energy state, so this pathway can be safely neglected (for more details, see ref. 6b). Note that the driving force of the process,

common to **1** – **3**, is relatively mild (ca 0.30 eV) so that this process is inefficient at 77 K, in rigid matrix, where the charge-separated states are destabilized. The consequence is that **1** – **3** exhibit the usual ^{3}MLCT emission at 77 K, like **M** (**Table 2**).

Reductive photoinduced electron transfer (RPET). This mechanism is assumed to largely take advantage of highest-lying occupied MOs of the bridge (i.e., it would be promoted by superexchange mechanism dominated by the hole-transfer route), so its efficiency and rate are expected to increase on destabilizing such orbitals. An electron-transfer route for superexchange mediated RPET is less efficient due to its two-electron character or the involvement of high-energy virtual states.[6b] Inserting sterically hindering substituents on the biphenylene bridging unit decreases the conjugation within this linker so stabilizing HOMO bridge-component and increasing the energy of the virtual excited state involved in the hole-transfer route for superexchange-assisted electron transfer.[2] However, the rate constants of this process in the three molecular dyads are quite close (**Table 3**). As far as **1** and **2** are concerned, this also agrees with the fact that the HOMO energies for the "BL-A" **L1** and **L2** compounds corresponding to **1** and **2**, centered on the biphenylene moieties, are practically identical,[9d] most likely as a consequence of balanced effects between decreased conjugation due to the presence of encumbered substituents in the biphenylene framework (that would stabilize HOMO) and the σ-donor nature of the methyl substituents introduced (that should destabilize HOMO). Whereas no similar data is available for **3**, the balanced effects should also be effective for this species with a little supplementary destabilizing contribution of the third methyl subtituent, so justifying the small deviation for the rate constant of **3** in comparison to **1** and **2**. RPET is much faster than OPET in **1** – **3**, possibly because of thermodynamic reasons (see **Table 3**, ΔG for RPET is about -1.10 eV and ΔG for OPET is about -0.30 eV).

Charge recombination (CR). The rate constant for charge recombination is derived from RPET. CR depends on both electron- and hole-transfer superexchange, i.e. on both LUMO and HOMO bridge energies. On the basis of the trend in rate constants in going from **1** to **2** and **3** for SS-EnT and OPET, it is clear that electronic coupling between the two chromophores via the electron-transfer route for superexchange coupling decreases from **1** to **3**, as a consequence of destabilization of the bridge-supported LUMO extension. The slow down of the charge recombination process on moving from **1** to **2** (15 ps vs 32 ps) tends to indicate that the electron transfer route dominates the superexchange coupling, at least for **1** and **2**. However, whereas the OPET and SS-EnT rate constants further decrease on passing to **3**, rate constant for CR remains the same on passing from **2** to **3** (**Table 3**). This points out that on increasing the number of methyl substituents, the hole-transfer route can have a role and could balance the decreased coupling via the electron-transfer pathway.

Charge recombination warrants an extra comment insofar as results from pump-probe experiments using 400 nm light as the pump are fully consistent with the established impossibility of accumulating charge-separated states via OPET, even though measured CR time constants are larger than those found for the photoinduced charge separation process as derived from the analysis of RPET. In fact, the forward charge separation processes (time constants of 40 ps, 173 ps, and 360 ps for **1**, **2**, and **3**, respectively) of the oxidative photoinduced pathway are slower than charge recombination, made available via the RPET processes (time constants of 15 ps for **1** and of 32 ps for **2** and **3**). Strictly speaking, however, the charge-separated states produced via oxidative and reductive photoinduced electron transfer (OPET and RPET) are not exactly the same states since, in the present case, RPET that involves a *singlet* excited state should lead to a *singlet* CS state (^{1}CS), whereas OPET, involving a *triplet* excited state, would lead to a *triplet* CS state (^{3}CS). Beyond any consideration on their relative energies (^{3}CS should be slightly lower in energy than ^{1}CS), charge recombination, leading to a singlet ground state, would be a spin-forbidden process for

^{3}CS and a spin-allowed one for ^{1}CS. In other covalently-linked systems a similar situation was considered and changes in rate constants for charge recombination involving singlet and triplet charge-separated states have been calculated and/or measured.[20,21] In such cases, it appeared that the differences between spin-allowed and spin-forbidden CR processes are not obvious, and energetic factors connected with Marcus theory should also be considered and can play a major role with respect to spin rules.[20] In some cases, large rate constants differences have been reported in favor of spin-allowed CR, but the spin-allowed route was there activated by an incoherent mechanism,[22] which is excluded in our case. In the present case, we have no possibility of calculating CR from the ^{3}CS, therefore, even if the effective time constants of the charge recombination involving the triplet state are not exactly the time constants measured for the singlet CS state, apparently they are anyway faster than the OPET process. This indicates that CR rate constants from ^{3}CS and ^{1}CS could be relatively small for **1** – **3**. As a very final consideration, since a heavy metal center is present in **1-3**, fast intersystem crossing between ^{1}CS and ^{3}CS can occur, so we can deal with ^{3}CS as the final state of excitation both via OPET and RPET in the present case.

Conclusions

Three new linearly-arranged multicomponent, bichromophoric systems **1** – **3** have been prepared and their rich photophysical properties have been studied, including by means of pump-probe transient absorption spectroscopy. The three compounds contain the same chromophores, that is a Ru(II)-terpy-like and a fused expanded bipyridinium (FEBP) subunits, separated by three different biphenylene-type brigdes. In all the new species, photoinduced energy and electron transfer processes take place, so quenching the emission of the components. The chromophores have been selected to be selectively addressable and excitation involving the Ru-based or the FEBP-based dyes results in different excited-state decays. Upon Ru-based excitation at 570 nm, *oxidative* photoinduced electron transfer

(OPET) takes place in **1** – **3** from the ^{3}MLCT state, however the charge-separated species does not accumulate, indicating that the charge recombination rate constant exceeds OPET rate constant. Upon excitation of the organic dye at 400 nm, the FEBP-based $^1\pi$–π^* level is prepared, which undergoes a series of intercomponent decay events, including (i) Dexter electron-exchange energy transfer leading to the MLCT manifold (SS-EnT), which successively decay according to 570 nm excitation, and (ii) *reductive* photoinduced electron transfer (RPET), leading to the preparation of the charge-separated (CS) state, formally a Ru^+-BL-A^- state (for simplicity, here Ru and A stand for the Ru-based and FEBP-based chromophores, respectively, and BL represents the biphenylene spacers). The reductive photoinduced charge separation, involving the FEBP singlet state, is much faster than the oxidative photoinduced charge separation, involving the MLCT triplet state, essentially because of driving force reasons, and this allows accumulation of the charge-separated state when FEBP-based subunit is excited, since the rate constant for CR, in all **1** – **3**, is intermediate between the rate constants of OPET and RPET. This peculiar situation makes **1** – **3** capable to selectively read the 400 nm excitation as an active input to prepare the CS state, whereas visible excitation at wavelengths longer than 480 nm is inefficient to accumulate the CS state.

Moreover, intriguing differences between the rate constants of the various processes in **1** – **3** have been analyzed and interpreted according to the superexchange theory for electron transfer. This allowed revealing the role of the electron-transfer and hole-transfer superexchange pathways in promoting the various intercomponent photoinduced processes occurring in **1** – **3**.

EXPERIMENTAL SECTION

Materials, syntheses of organic ligands and related inorganic dyads, along with full characterizations are provided in the Supporting Information. Electrochemical experiments were carried out with a conventional three-electrode cell and a PC-controlled potentiostat/galvanostat (Princeton Applied Research Inc. model 263A). The working electrode was a platinum electrode from Radiometer-Tacussel (area, 0.0314 cm^2; diameter, 2.0 mm) mounted on Teflon. Platinum wire was used as the counter-electrode and a saturated calomel electrode (SCE) as the reference. Electrolytic solutions, MeCN (Aldrich, anhydrous, 99.8%) containing 0.1 M tetrabutylammonium hexafluorophosphate ($TBAPF_6$, Aldrich, +99%) as a supporting electrolyte, were routinely deoxygenated by argon bubbling. All potential values are given versus the SCE. Further information is given in the Supporting Information. UV/Vis absorption spectra were taken on a Jasco V-560 spectrophotometer. For steady-state luminescence measurements, a Jobin Yvon-Spex Fluoromax P spectrofluorimeter was used, equipped with a Hamamatsu R3896 photomultiplier. The spectra were corrected for photomultiplier response using a program purchased with the fluorimeter. For the luminescence lifetimes, an Edinburgh OB 900 time-correlated single-photon-counting spectrometer was used. As excitation sources, a Hamamatsu PLP 2 laser diode (59 ps pulse width at 408 nm) and/or the nitrogen discharge (pulse width 2 ns at 337 nm) were employed. Time-resolved transient absorption experiments were performed using a pump-probe setup based on the Spectra-Physics MAI-TAI Ti:sapphire system as the laser source and the Ultrafast Systems Helios spectrometer as the detector. The output of laser beam was split to generate pump and probe beam pulses with a beam splitter (85 and 15%). The pump pulse (400 nm, 1-2 μJ) was generated with a Spectra-Physics 800 FP OPA and was focused onto the sample cuvette. The probe beam was delayed with a computer controlled motion controller and then focused into a 2-mm sapphire plate to generate a white light continuum (spectral range 450–800 nm). The white light is then overlapped with the pump beam in a 2-mm quartz cuvette containing the

sample. The effective time resolution was ca. 200 fs, and the temporal chirp over the white-light 450–750 nm range ca. 150 fs; the temporal window of the optical delay stage was 0–3200 ps. The time-resolved data were analyzed with the Ultrafast Systems Surface Explorer Pro software. More information are given in the Supporting Information.

Experimental uncertainties are as follows: redox potential values, 10 mV; absorption maxima, 2 nm; luminescence maxima, 4 nm; luminescence lifetimes, 10%; luminescence quantum yields, 15%; transient absorption decay and rise rates, 10%.

ASSOCIATED CONTENT

Supporting Information. Experimental details for the synthesis and characterization of new compounds and precursors including ^{1}H NMR (500 MHz) and ^{13}C NMR (126 MHz) spectra as well as ESI mass spectra; absorption spectra of **L0**, **L0a**, **L1, L2**, **1** and **2**; transient absorption spectra matrices of **M**, **1**, **2** and **3**. This material is available free of charge via the Internet at http://pubs.acs.org.

AUTHOR INFORMATION

Corresponding authors

*E-mail: fpuntoriero@unime.it.

*E-mail: campagna@unime.it.

*E-mail: philippe.laine@univ-paris-diderot.fr.

Notes

The authors declare no competing financial interest.

ACKNOWLEDGMENTS

Financial support by the French National Research Agency, ANR ("E-StorIc" project : ANR-14-CE05-0002), is gratefully acknowledged by F.T., G.D., and P.P.L.. The Italian Ministero degli Affari Esteri e per la Cooperazione Internazionale (MAECI) is acknowledged by S.C., A. S., and G.L.G.. F.P. thanks the University of Messina for FFABR program.

References and Notes

1 The literature on this topic is too vaste to be exhaustevely quote. For some representative examples, see: (a) Sauvage, J.-P.; Collin, J.-P.; Chambron, J. C.; Guillarez, S.; Coudret, C.; Balzani, V.; Barigelletti, F.; De Cola, L.; Flamigni, L. Ruthenium(II) and Osmium(II) Bis(terpyridine) Complexes in Covalently-Linked Multicomponent Systems: Synthesis, Electrochemical Behavior, Absorption Spectra, and Photochemical and Photophysical Properties. *Chem. Rev.*, **1994**, *4*, 993. (b) Balzani, V.; Campagna, S.; Denti, G.; Juris, A.; Serroni, S.; Venturi, M. Designing Dendrimers Based on Transition-Metal Complexes. Light-Harvesting Properties and Predetermined Redox Patterns. *Acc. Chem. Res.*, **1998**, *31*, 26. (c) Fleming, C. N.; Maxwell, K. A.; DeSimone, J. M.; Meyer, T. J.; Papanikolas, J. M. Ultrafast Excited-State Energy Migration Dynamics in an Efficient Light-Harvesting Antenna Polymer Based on Ru(II) and Os(II) Polypyridyl Complexes. *J. Am Chem. Soc.*, **2001**, *123*, 10336. (d) Alstrum-Acevedo, J. H.; Brennaman, M. K.; Meyer, T. J. Chemical Approaches to Artificial Photosynthesis. 2. *Inorg. Chem.*, **2005**, *44*, 6802. (e) Balaban, T. S. Tailoring Porphyrins and Chlorins for Self-Assembly in Biomimetic Artificial Antenna Systems. *Acc. Chem. Res.* **2005**, *38*, 612. (f) Aratani, N.; Kim, D.; Osuka, A. Discrete Cyclic Porphyrin Arrays as Artificial Light-Harvesting Antenna. *Acc. Chem. Res.*, **2009**, *42*, 1922. (g) Wasielewski, M. R. Self-Assembly Strategies for Integrating Light Harvesting and Charge Separation in Artificial Photosynthetic Systems. *Acc. Chem. Res.*, **2009,** *42*, 1910, and refs. therein. (h) Gust, D.; Moore, T. A.; Moore, A. L. Solar Fuels via Artificial Photosynthesis. *Acc. Chem. Res.*, **2009**, *42*, 1890, and refs. therein. (i) Rickhaus, M.; Jentzsch, A. V.; Tejerina, L.; Grübner, I.; Jarisek, M.; Claridge, T. D. W.; Andersson, H. L. Single-Acetylene Linked Porphyrin Nanorings. *J. Am. Chem. Soc.*, **2017**, *139*, 16502. (j) Kent, C. A.; Mehl, B. P.; Papanikolas, J. M.; Meyer, T. J.; Lin, W. Energy Transfer Dynamics in Metal−Organic Frameworks. *J. Am Chem. Soc.*, **2010**,

132, 12767. (k) Stadler, A.-M.; Puntoriero, F.; Nastasi, F.; Campagna, S.; Lehn, J.-M. Ru^{II} Multinuclear Metallosupramolecular Rack‐Type Architectures of Polytopic Hydrazone‐Based Ligands: Synthesis, Structural Features, Absorption Spectra, Redox Behavior, and Near‐Infrared Luminescence. *Chem. Eur. J.*, **2010**, *16*, 5645. (l) Shi, Y.; Sanchez-Molina, I.; Cao, C.; Cook, T. R.; Stang, P. J. Synthesis and photophysical studies of self-assembled multicomponent supramolecular coordination prisms bearing porphyrin faces. *Proc. Natl. Acad. Sci*, **2014**, *111*, 9390.

2 For some representative examples, see: (a) Balzani, V.; Scandola, F. *Supramolecular Photochemistry*, Horwood, Chichester, UK, 1991. (b) Danielson, E.; Elliott, C. M.; Merkert, J. W.; Meyer, T. J. Photochemically induced charge separation at the molecular level. A chromophore-quencher complex containing both an electron donor and an acceptor. *J. Am. Chem. Soc.*, **1987**, *109*, 2519. (c) Meyer, T. J. Chemical approaches to artificial photosynthesis. *Acc. Chem. Res.*, **1989**, *22*, 163. (d) Wasielewki, M. R. Photoinduced electron transfer in supramolecular systems for artificial photosynthesis. *Chem. Rev.*, **1992**, *92*, 435, and refs. therein. (e) Gust, D.; Moore, T. A.; Moore, A. L. Molecular mimicry of photosynthetic energy and electron transfer. *Acc. Chem. Res.*, **1993**, *26*, 198, and refs. therein. (f) Paddon-Row, M. N. Investigating long-range electron-transfer processes with rigid, covalently linked donor-(norbornylogous bridge)-acceptor systems. *Acc. Chem. Res.*, **1994**, *27*, 18. (g) Beratan, D. N.; Skourtis, S. S. Electron transfer mechanisms. *Curr. Op. Chem. Biol.*, **1998**, *2*, 235. (h) Kumaresan, D.; Lebrowsky, K.; Schmehl, R. H. Photoinduced charge separation and recombination in solution and in gels of a Pt(II) terpyridyl–naphthalene diimide complex. *I. Photochem. Photobiol. A: Chem.*, **2009**, *207*, 86. (i) Albinsson, B.; Martensson, J. Long-range electron and excitation energy transfer in donor–bridge–acceptor systems. *J. Photochem. Photobiol. C: Photochem. Rev.*, **2008**, *9*, 138, and refs. therein. (j) Natali, M.; Ravaglia, M.; Scandola, F.; Boixel, J.; Pellegrin, Y.; Blart, E.; Odobel, F. Long-

Range Charge Separation in a Ferrocene-(Zinc Porphyrin)–Naphthalenediimide Triad. Asymmetric Role of 1,2,3-Triazole Linkers. *J. Phys. Chem. C*, **2013**, *117*, 19334. (k) Winkler, J. R.; Gray, H. B. Electron Flow through Metalloproteins. *Chem. Rev.*, **2014**, *114*, 3369. (l) Guldi, D.; Fukuzumi, S. Electron transfer in electron donor-acceptor ensembles containing porphyrins and metalloporphyrins. *J. Porphyrins Phthalocyanines*, **2002**, *6*, 289. (m) Curutchet, C.; Feist, F. A.; Van Averbeke, B.; Mennucci, B.; Jacob, J.; Müllen, K.; Basché, T; Beljonne, D. Superexchange-mediated electronic energy transfer in a model dyad. *Phys. Chem. Chem. Phys.*, **2010**, *12*, 7378. (n) Jones, A. L.; Gish, M. K.; Zeman, C. J. IV; Papanikolas, J. L.; Schanze, K. S. Photoinduced Electron Transfer in Naphthalene Diimide End-Capped Thiophene Oligomers *J. Phys. Chem. A*, **2017**, *121*, 9579. (o) Gronheid, R.; Stefan, A.; Cotlet, M.; Hofkens, J.; Qu, J.; Müllen, K.; Van der Auweraer, M.; Verhoeven, J. W.; De Schryver, F. C. Reversible Intramolecular Electron Transfer at the Single‐Molecule Level *Angew. Chem. Int. Ed.*, **2003**, *42*, 4209. (p) Nomrowski, J.; Wenger, O. S. Exploiting Potential Inversion for Photoinduced Multielectron Transfer and Accumulation of Redox Equivalents in a Molecular Heptad. *J. Am. Chem. Soc.*, **2018**, *140*, 5343.

3 Balzani, V.; Credi, A.; Venturi, M. *Molecular Devices and Machines - Concepts and Perspectives for the Nanoworld, 2nd Edition*, Wiley-VCH, Weinheim, 2008.

4 (a) Lehn, J.-M. Toward complex matter: Supramolecular chemistry and self-organization. *Proc. Natl. Acad. Sci.*, **2002**, *99*, 4763. (b) Lehn, J.-M. *Supramolecular Chemistry – Concepts and Perspectives*, Wiley-VCH, Weinheim, 2006.

5 This is different from the trivial case of a bichromophoric species in which the two (different) chromophores do not exhibit any interaction one another, so they emit separately and independently.

6 (a) Arrigo, A.; Santoro, A.; Indelli, M. T.; Natali, M.; Scandola, F.; Campagna, S. On the effect of the nature of the bridge on oxidative or reductive photoinduced electron

transfer in donor–bridge–acceptor systems. *Phys. Chem. Chem. Phys.*, **2014**, *16*, 818. (b) Natali, M.; Campagna, S.; Scandola, F. Photoinduced electron transfer across molecular bridges: electron- and hole-transfer superexchange pathways. *Chem. Soc. Rev.*, **2014**, *43,* 4005, and refs. therein.

7 (a) Walther, M. E; Wenger, O. S. Hole Tunneling and Hopping in a Ru(bpy)32+-Phenothiazine Dyad with a Bridge Derived from oligo-p-Phenylene *Inorg, Chem.*, **2011**, *50*, 10901. (b) Indelli, M. T.; Orlandi, M.; Chiorboli, C.; Ravaglia, M.; Scandola, F.; Lafolet, F.; Welter, S.; De Cola, L. Electron Transfer Across Modular Oligo-p-phenylene Bridges in $Ru(bpy)_2(bpy–ph_n–DQ)^{4+}$ (n = 1–5) Dyads. Unusual Effects of Bridge Elongation. *J. Phys. Chem. A*, **2012**, *116*, 119. (c) Fortage, J.; Puntoriero, F.; Tuyèras, F.; Dupeyre, G.; Arrigo, A.; Ciofini, I.; Lainé, P. P.; Campagna, S. Photoinduced Electron Transfers in Osmium(II)(terpyridine)-Biphenylene-(Bi)pyridinium Assemblies. *Inorg. Chem.*, **2012**, *51*, 5342. (d) Gilbert, M.; Albinsson, B. Photoinduced charge and energy transfer in molecular wires. *Chem. Soc. Rev.*, **2015**, *44*, 845.

8 Paddon-Row, M. N. In *Electron Transfer in Chemistry* (Ed. Balzani, V.), Wiley-VCH, Weinheim, 2001, Vol. 3, 179.

9 (a) Fortage, J.; Tuyèras, F.; Ochsenbein, P.; Puntoriero, F.; Nastasi, F.; Campagna, S.; Griveau, S.; Bedioui, F.; Ciofini, I.; Lainé, P. P. Expanded Pyridiniums: Bis-cyclization of Branched Pyridiniums into Their Fused Polycyclic and Positively Charged Derivatives – Assessing the Impact of Pericondensation on Structural, Electrochemical, Electronic and Photophysical Features. *Chem. Eur. J.*, **2010**, *16*, 11047. (b) Fortage, J.; Peltier, C.; Nastasi, F.; Puntoriero, F.; Tuyèras, F.; Griveau, S.; Bedioui, F.; Adamo, C.; Ciofini, I.; Campagna, S.; Lainé, P. P. Designing Multifunctional Expanded Pyridiniums: Properties of Branched and Fused *Head-to-Tail* Bipyridiniums. *J. Am. Chem. Soc.*, **2010**, *132*, 16700. (c) Peltier, C.; Adamo, C.; Lainé, P. P.; Campagna, S.;

Puntoriero, F.; Ciofini, I. Theoretical Insights into Branched and Fused Expanded Pyridiniums by the Means of Density Functional Theory. *J. Phys. Chem. A*, **2010,** *114***,** 8434. (d) Fortage, J.; Tuyeras, F.; Peltier, C.; Dupeyre, G.; Calborean, A.; Bedioui, F.; Ochsenbein, P.; Puntoriero, F.; Campagna, S.; Ciofini, I.; Lainé, P. P. Tictoid Expanded Pyridiniums: Assessing Structural, Electrochemical, Electronic and Photophysical Features. *J. Phys. Chem. A*, **2012**, *116*, 7880. (e) Fortage, J.; Dupeyre, G.; Tuyèras, F.; Marvaud, V.; Ochsenbein, P.; Ciofini, I.; Hromadová, M.; Pospísil, L.; Arrigo, A.; Trovato, E.; Puntoriero, F.; Lainé, P. P.; Campagna, S. Molecular Dyads of Ru(II)– or Os(II)–Bis(terpyridine) Chromophores and Expanded Pyridinium Acceptors. Equilibration between MLCT and Charge-Separated Excited States. *Inorg. Chem.*, **2013**, *52*, 11944.

10 (a) Fortage, J.; Peltier, C.; Perruchot, C.; Takemoto, Y.; Teki, Y.; Bediou, F.; Marvaud, V.; Dupeyre, G.; Pospisil, L.; Adamo, C.; Hromadova, M.; Ciofini, I.; Lainé, P. P. Single-Step versus Stepwise Two-electron Reduction of Polyarylpyridiniums: Insights from the Steric Switching of Redox Potential Compression. *J. Am. Chem. Soc.*, **2012**, *134*, 2691. (b) Lachmanova, S.; Dupeyre, G.; Tarabek, J.; Ochsenbein, P.; Perruchot, C.; Ciofini, I.; Hromadova, M.; Pospisil, L.; Lainé, P. P. Kinetics of Multielectron Transfers and Redox-Induced Structural Changes in *N*-Aryl-Expanded Pyridiniums: Establishing Their Unusual, Versatile Electrophoric Activity. *J. Am. Chem. Soc.*, **2015**, *137*, 11349.

11 (a) Meyer, T. J. Photochemistry of metal coordination complexes: metal to ligand charge transfer excited states. *Pure Appl. Chem.*, **1986**, *58*, 1193. (b) Juris, A.; Balzani, V.; Barigelletti, F.; Campagna, S.; Belser, P.; von Zelewsky, A. Ru(II) Polypyridine Photochemistry, Electrochemistry and Chemiluminescence, *Coord. Chem. Rev.* **1988**, *84*, 85. (c) Campagna, S.; Puntoriero, F.; Nastasi, F.; Bergamini, G.; Balzani, V. Photochemistry and Photophysics of Coordination Compounds: Ruthenium. *Top. Curr. Chem.,* **2007***, 280*, 117.

12 Of note, the electronic absorption spectrum of organic FEBP-based units does not change appreciably with the change of the methyl-substitution pattern of its pendant biphenylene group as a proto-spacer, see ref. **9d**.

13 The discussion assumes that Koopman theorem (Koopman, T. *Physica*, **1934**, *1*, 104) is valid.

14 Lainé, P. P.; Campagna, S.; Loiseau, F. Conformationally Gated Photoinduced Processes within Photosensitizer – Acceptor Dyads Based on Ruthenium(II) and Osmium(II) Polypyridyl Complexes with an Appended Pyridinium Group. *Coord. Chem. Rev*. **2008**, *252*, 2552.

15 (a) McCusker, J. K. Femtosecond absorption spectroscopy of transition metal charge-transfer complexes. *Acc. Chem. Res.*, **2003**, *36*, 876. (b) Chergui, M. Ultrafast Photophysics of Transition Metal Complexes. *Acc. Chem. Res.*, **2015,** *48***,** 801.

16 (a) McConnell, H. M. Theory of Isotropic Hyperfine Interactions in π - Electron Radicals. *J. Chem. Phys.*, **1961**, *35*, 508. (b) Kornyshev, A. A.; Kuznetsov, A. M.; Ulstrup, J. In situ superexchange electron transfer through a single molecule. *Proc. Natl. Acad. Sci.*, **2006,** *103*, 6799.

17 Arrigo, A.; Santoro, A.; Puntoriero, F.; Lainé, P. P.; Campagna, S. Photoinduced electron transfer in donor-bridge-acceptor assemblies: the case of Os(II)-bis(terpyridine)-(bi)pyridinium dyads. *Coord. Chem. Rev.,* **2015**, *304-305*, 109.

18 The value of 0.34 eV is a low-limit for the singlet-singlet energy transfer, since the energy of the singlet MLCT state is lower than its absorption band maximum, however it can be accepted for this level of approximation and for our aims.

19 In equations 5 and 6, ken is the rate constant of the energy transfer process, K is orientation factor which accounts for the directional nature of the dipole-dipole interaction (K is 2/3 for random orientation), Φ and τ are the luminescence quantum yield and lifetime of the donor, respectively, n is the solvent refractive index, r_{AB} is the

distance between donor and acceptor (13 Å for all the species, evaluated from energy minimized computed structures), and J_F is the Foerster overlap integral between the luminescence spectrum of the donor, F(v), and the absorption spectrum of the acceptor, ε (v), on an energy scale (cm^{-1}). For **1** J_F is 2.095 x 10^{-14} cm^6, and for both **2** and **3** is 3.93 x 10^{-14} cm^6.

20 (a) Verhoeven, J. W. On the role of spin correlation in the formation, decay, and detection of long-lived, intramolecular charge-transfer states. *J. Photochem. Photobiol. C: Photochem. Rev.*, **2006**, *7*, 40. (b) Rawls, M. T.; Kollmannsberger, G.; Elliott, C. M.; Steiner, U. E. Spin relaxation in Ru-chromophore-linked azine/diquat radical pairs. *J. Phys. Chem. A*, **2007**, *111*, 3485.

21 (a) Weiss, E. A.; Tauber, M. J.; Kelley, R. F.; Ahrens, M. J.; Ratner, M. A.; Wasielewski, M. R. Conformationally gated switching between superexchange and hopping within oligo-p-phenylene-based molecular wires. *J. Am. Chem. Soc.,* **2005**, *127*, 11842. (b) Miura, T.; Scott, A. M.; Wasielewski, M. R. Electron Spin Dynamics as a Controlling Factor for Spin-Selective Charge Recombination in Donor-Bridge-Acceptor Molecules. *J. Phys. Chem. C*, **2010**, *114*, 20370.

22 Fay, P. T.; Lewis, A. M.; Manolopoulos, D. E. Spin-dependent charge recombination along para-phenylene molecular wires. *J. Chem. Phys.* **2017**, *147,* 064107.

TABLE OF CONTENTS - GRAPHICS AND SYNOPSIS

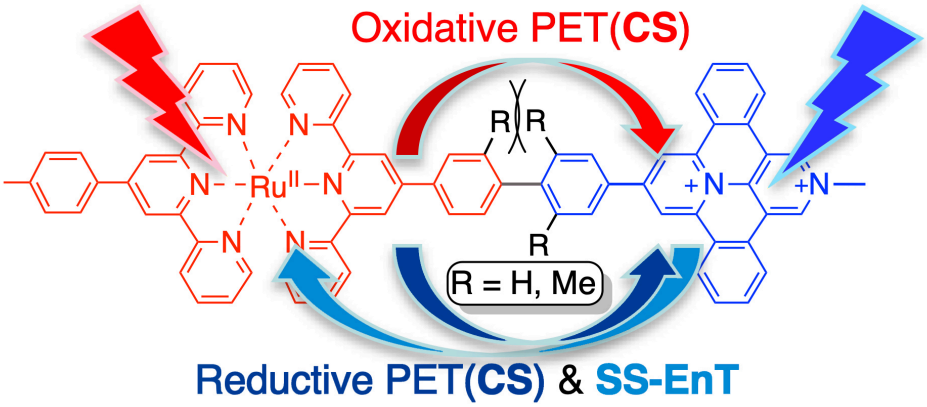

Three linearly-arranged bichromophoric systems undergo different excited-state decay processes when selectively excited, with charge-separated state accumulated only when the organic chromophore is addressed. Superexchange allows to rationalize rate constants and excited-state routes, involving Dexter energy transfer and oxidative or reductive electron transfer, along the series.